International Journal of Innovative Computing, Information and Control
Volume **14**, Number **1**, February **2018**
 ISSN 1349-4198
pp. **227–241**

AN ITERATIVE DIRECTION FINDING ALGORITHM WITH ULTRA-SMALL APERTURES

Rong Fan[1], Wensheng Qiao[1], Li Wang[1], Yang Liu[2] and Xueke Ding[3]

[1]CETC Key Laboratory of Avionic Information System Technology
China Electronics Technology Group Corporation
No. 85, Yingkang West Road, Chengdu 610036, P. R. China
fanrong@alu.uestc.edu.cn

[2]School of Electronic Engineering
University of Electronic Science and Technology of China
No. 2006, Xiyuan Ave., West Hi-Tech Zone, Chengdu 611731, P. R. China

[3]Tongfang Electronic Science and Technology Co., Ltd
No. 111, Ruichang Avenue, Jiujiang 332000, P. R. China

Received April 2017; revised August 2017

Abstract. *In array direction finding system, the accuracy of angle measurement is determined by the ratio of array aperture to the wavelength of sources and non-ideal factors, such as the channel gain and phase errors, mutual coupling errors as well as the element pattern errors. These non-ideal factors must be calibrated for any practical direction finding system. Besides, to obtain an acceptable angle measurement accuracy, a large array aperture size is required with traditional method. In view of the drawback of traditional method, an iterative direction finding method with ultra-small aperture which is based on the sample database (namely, IDFA-USA) is proposed in the paper. With the proposed method, a better DOA estimation performance than the traditional method's is obtained. Finally, computer simulation results illustrate advantages of the proposed method.*
Keywords: Direction finding, Ultra-small aperture, Correlation interferometer, Iterative algorithms

1. **Introduction.** As one of the most important fields in the array signal processing (ASP), the direction finding (DF) has attracted wide attention of researchers and engineers. It has been widely used in radar imaging, wireless communication and radio spectrum detection [1, 2, 3].

Up to now, there are three categories of angle measurement technologies: the amplitude comparison direction finding (DF) based on the amplitude information of the array output [4, 5], the interferometer based on the phase information of the array output [6, 7], and the spatial spectrum direction finding exploiting both the amplitude and phase information [8, 9]. As a matter of fact, DF systems can also be divided into large aperture systems, medium aperture systems and small aperture systems based on the ratio of array aperture to signal wavelength. Similarly, we further define the ultra-small aperture systems. The specified definitions are shown in Table 1. In practical DF platform, the array aperture is restricted extremely such as UAV platform, and missile. It is unrealistic to obtain an acceptable accuracy with existing methods. So, it is important to develop an alternative DF algorithm for ultra-small aperture. Although several DF algorithms have been reported on previous works, these algorithms are developed to estimate the DOA for underwater environment and it is beyond out scope of this paper [10, 11]. For the radio DF issue in the air, as far as our best knowledge, there is no publication on the ultra-small aperture

TABLE 1. Array aperture specification

Large Aperture	Medium Aperture	Small Aperture	Ultra-Small Aperture
$L \geq \lambda$	$\lambda \leq L < 2\lambda$	$0.3\lambda < L < \lambda$	$L \leq 0.3\lambda$

direction finding issue until now. To fill this technical gap, we propose a DF method which is suitable for ultra-small aperture scenario. The contributions of this paper are: firstly, the proposed method exploits both magnitude and phase features of element pattern and channel inconsistences of receiver to construct feature database, rather than correct the non-ideal errors of DF systems. It must have to correct the non-ideal errors with most existing DF methods. Second, the proposed method is insensitive to the array aperture size, so we can obtain the acceptable accuracy with ultra-small aperture. Thirdly, since we relax the restriction of DF platform size, the range of applications is also expanded.

This paper is organized as follows. Problem formulation of the ultra-small aperture direction finding system is presented in Section 2. The proposed DF method for the ultra-small aperture system is discussed in Section 3. Section 4 shows simulations and verifications. Finally, the summary of the paper is presented in Section 5. In this paper, the scalar signal, vector signal and matrix signal are represented by lower case letters, bold lower case letters and upper bold case letters, respectively.

2. Problem Formulation.

2.1. The ultra-small aperture DF system signal model.

For simplicity, consider a narrow band plane wave at direction θ impinges on a linear array composed of M elements. In order to facilitate the description, the antenna array elements in Figure 1 are denoted by $1\# \sim M\#$ from left to right. Without loss of generality, the $1\#$ element is used as the reference and the coordinates in the Cartesian coordinate system are zero. The source and the noise, as well as the noise between elements are independent. The m-th noise-corrupted element output is denoted by

$$x_m(t) = a_m(\theta)s(t) + n_m(t) \quad m = 1, 2, \ldots, M \tag{1}$$

In Equation (1), $s(t)$ is the waveform of source. And a_m is defined as follows

$$a_m(\theta) = g_m(\theta) \exp(-j2\pi d_m \sin(\theta)/\lambda) \tag{2}$$

In Equation (2), $g_m(\theta)$ is the complex gain of the m-th element at angle θ. λ is the wavelength of signal. d_m is the distance from the m-th element to the reference element. $n_m(t)$ is the additive white Gaussian noise of the m-th element with zero mean and variance σ^2 (namely, $n_m(t) \sim N[0, \sigma^2]$).

This scenario can be described by the following signal model

$$\mathbf{x}(t) = \mathbf{a}s(t) + \mathbf{n}(t) \tag{3}$$

where

$$\mathbf{a}(\theta) = [a_1(\theta), a_2(\theta), \ldots, a_M(\theta)]^T \tag{4}$$

As the signal model can be extended to multiple sources scenarios straightly, we only present single source DF signal model in the paper. To obtain better accuracy, the aperture size should be multiple times larger than the wavelength in the existing DF system.

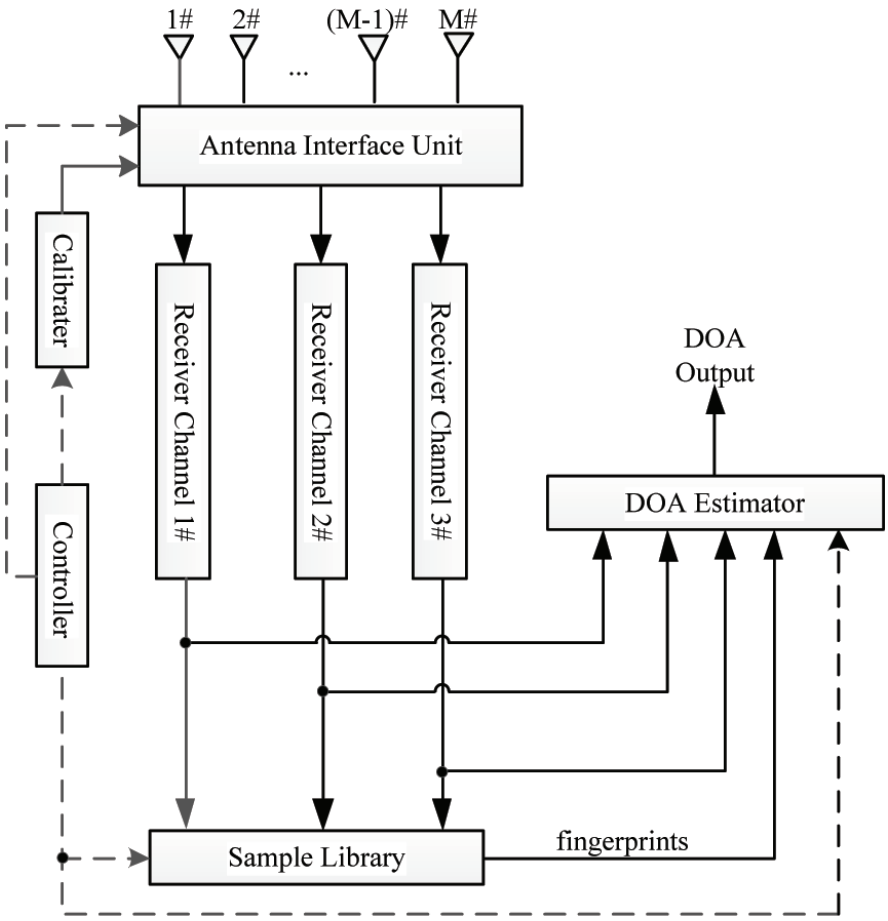

FIGURE 1. The ultra-small aperture direction finding system

2.2. **Flow diagram of the ultra-small DF system.** In the correlation interferometer DF system, DOA is calculated by the correlation coefficient w.r.t. angles. Correlation coefficient is calculated using the phase difference stored in sample library and the measured phase difference.

The ultra-small aperture DF system is shown in Figure 1. Different from the existing correlation interferometer [12], three of array elements are selected through the antenna interface unit (AIU) according to predefined selection strategies in the ultra-small DF system. Meanwhile, sample library building unit, calibrator, 3-channel receivers, and DOA estimator are coordinated by the controller. The DF procedures are divided into three stages: Firstly, to establish sample database (namely, establishing the feature database w.r.t. the angle). A known signal source from the far field is placed at each angle position. Based on the predefined selecting strategy, samples measured by 3-channel receiver are stored in the sample library building unit, which contains all non-ideal errors (such as magnitude errors, and phase errors). Secondly, to determine the DOA of sources, phase differences of elements are calculated with the same selecting strategy as the sample database establishment phase. In this process, correlation coefficients are carried out using the sample database and the measured array outputs of the signal. Thirdly, to calibrate the DF system period, according to a specified time interval, DF task is interrupted by controller to update the sample library. The flow diagram of the ultra-small aperture system is shown in Figure 2.

As shown in the figure, the whole direction finding flow is divided into three parts: the establishment of fingerprint sample library, the realization of direction finding function

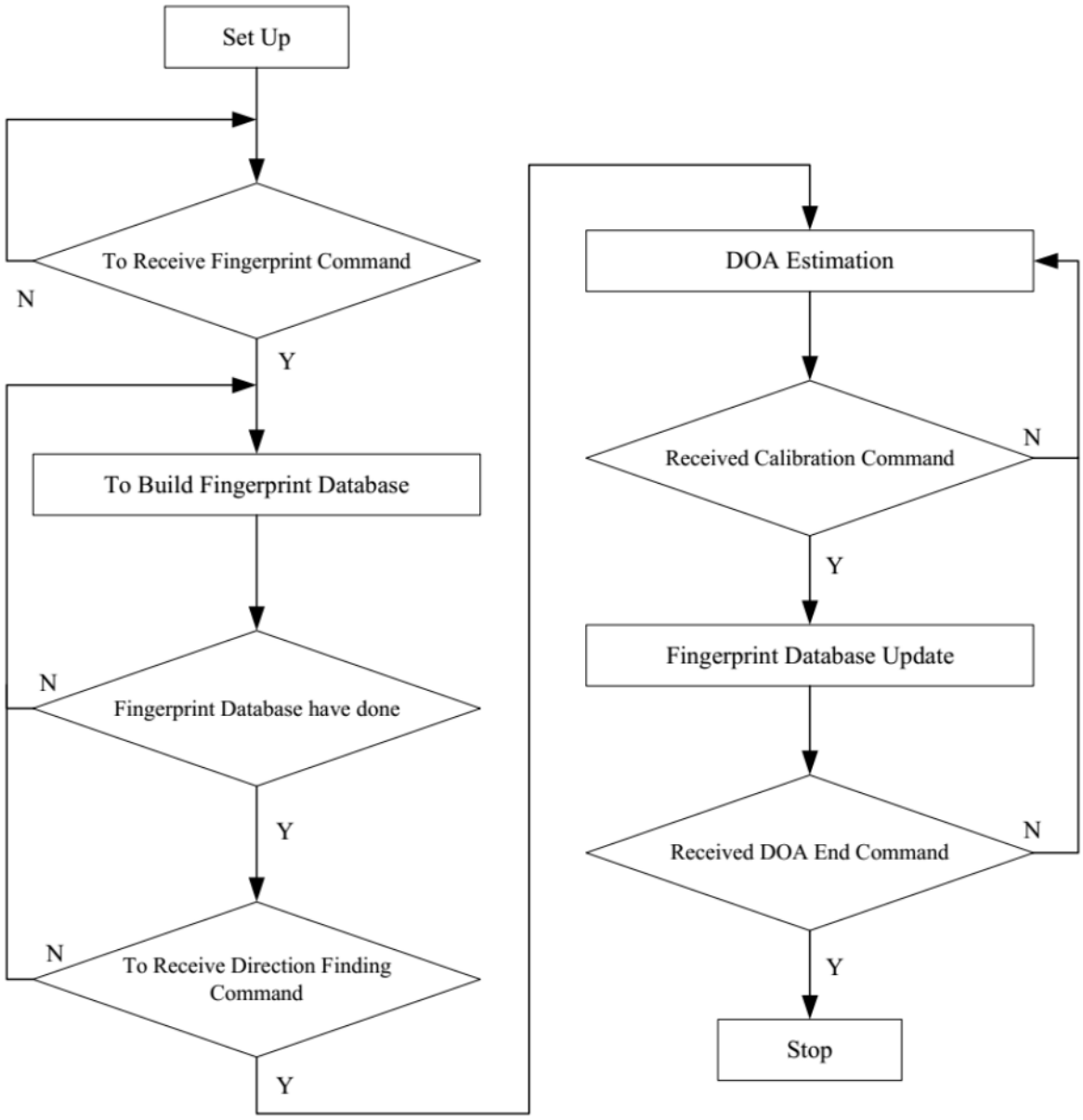

FIGURE 2. The DF flow diagram of the ultra-small aperture system

and the cycle updating of channel errors. The task in the first part is to extract sample fingerprints, which includes both mutual coupling of antenna and antenna pattern at all angles and frequency bands (Both range of angles and frequency band are presignified by designer). It should be noted that the system channel non ideal factors of the DF system must be eliminated. The task in the second part is mainly to perform DOA estimation. Because DF system is inevitably influenced by external environment (such as temperature, humidity, start-up and shutdown), magnitude-phase errors between channels are varied with time. In order to ensure the DOA estimation performance, in the stage of the cycle updating of channel errors, it is critical to update the channel errors periodically.

Remark 2.1. *It should be noted that the 3-channel receiver system used in this paper is not the only choice. As a matter of fact, 2-channel, 4-channel as well as 5-channel receiver DF systems are also suitable to our method. With more channels receiver system, better DOA performance can be obtained. However, receivers with more channels will lead to increasing the cost and complexity of the system. There is a trade-off between the number*

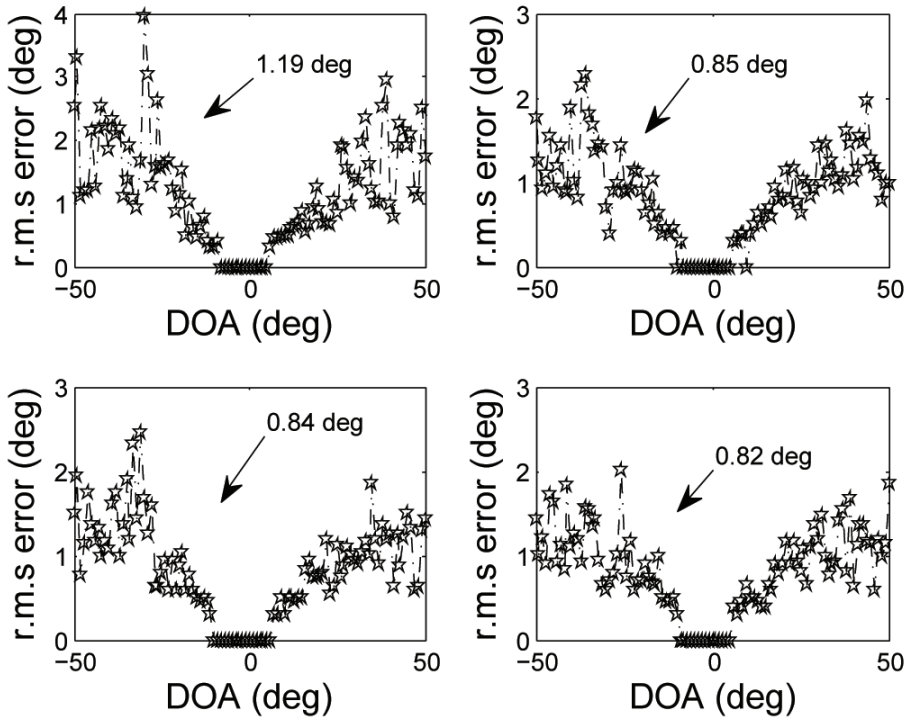

FIGURE 3. DOA performance with 2-channel receiver (upper left), 3-channel receiver (upper right), 4-channel receiver (lower left), 5-channel receiver (lower left)

of channels and DOA performance. In this paper, 2-channel, 3-channel, 4-channel, as well well as 5-channel receiver systems were simulated, respectively. Simulation results are shown in Figure 3. Results show that the DOA performance improvement is ignored with more than 3-channel receiver system. Therefore, a 3-channel receiver system is adapted in this article (In simulation, the parameters are exactly the same in Experiment 1).

3. **The Ultra-Small Aperture Array DOA Realization.**

3.1. **Establishment of feature database.** Firstly, we denote the feasible DOA range of source and the discrete interval by $\theta_{\min} \sim \theta_{\max}$ and $\Delta\theta$ respectively. For linear array, the minimum value of $\theta_{\min}$ and the maximum value of $\theta_{\max}$ can be taken as -90 and 90 degree, respectively. DOA range is divided into L discrete angle

$$L = \left[\frac{\theta_{\max} - \theta_{\min}}{\Delta\theta}\right] \tag{5}$$

where $[\cdot]$ is the round operator. The three elements of arrays are defined as the combination of a selection. Without loss of generality, the k-th antenna assembly is

$$\mathbf{c}_k = \{c_{1,k}, c_{2,k}, c_{3,k}\} \tag{6}$$

where $\{\cdot\}$ is a set of elements.

$$1 \le c_{1,k} < c_{2,k} < c_{3,k} \le M, \quad c_{1,k}, c_{2,k}, c_{3,k} \in Z^+ \tag{7}$$

The antenna selection mode is specified by designer. For M elements, there are $M(M+1)/2$ combinations ($1 \le k \le M(M+1)/2$) in total. In this paper, we denote the k-th

atom by $c_k = \{c_{1,k}, c_{2,k}, c_{3,k}\}$. Meanwhile, the phase difference between elements in each atom is called atom fingerprint, which is denoted as

$$\mathbf{v}_k(\theta) = \{v_{1,k}(\theta), v_{2,k}(\theta), v_{3,k}(\theta)\} \tag{8}$$

Furthermore, multiple atoms arranged in specified order are reformulated as the molecular fingerprint. In the actual DF system, the number of atoms in a molecular fingerprint is determined according to the actual requirements. For the M elements, molecular fingerprints contain a maximum of $M(M+1)/2$ atomic fingerprints. In order to obtain a better ability of solving the fuzziness, we need more atoms in a molecular fingerprint; however, the computation complexity also increases. For the incident signal from far field at θ_i, we construct atomic fingerprints at the all possible directions of the target signal. The atomic fingerprint contains all errors, such as the position errors of antenna array installation, the mutual coupling errors among elements, the magnitude and phase errors among receivers.

Molecular fingerprints constructed by atomic fingerprints are reformulated as follows,

$$\gamma(\theta_i) = \left[\mathbf{v}_1(\theta_i), \mathbf{v}_2(\theta_i), \ldots, \mathbf{v}_{(M+1)M/2}(\theta_i)\right]^T \tag{9}$$

and the original samples are formed by Equation (9). $[\cdot]^T$ is the transpose operator.

3.2. **DOA principle for ultra-small aperture.** For an actual signal, the measured phase difference in specified order (by Equation (6)) is aligned as follows,

$$\hat{\gamma}(\theta_i) = \left[\hat{\mathbf{v}}_1(\theta_i), \hat{\mathbf{v}}_2(\theta_i), \ldots, \hat{\mathbf{v}}_M(\theta_i)\right]^T \tag{10}$$

The correlation coefficients are calculated by cross correlation operation between the measured phase difference $\hat{\gamma}(\theta_i)$ and the molecular fingerprint of the system $\hat{\gamma}(\theta_i)$. Angle location w.r.t. the maximum value of the correlation coefficient between the measured phase difference and the molecular fingerprint is the direction of the source, i.e.,

$$\hat{\theta} = \arg\max_{\theta_i} \frac{< \hat{\gamma}(\theta), \hat{\gamma}(\theta_i) >}{\|\hat{\gamma}(\theta)\|_2 \cdot \|\hat{\gamma}(\theta_i)\|_2} \quad \text{s.t. } \theta_i \in \left[\theta_{\min}, \theta_{\max}\right] \tag{11}$$

where $< \cdot >$ is the inner product operation. $\|\cdot\|_2$ is the l_2-norm. It must be pointed out that the available objective function is just one of the selectable ones. There are also several other choices such as Euclidean distance, and maximum entropy. However, different cost functions will lead to different DOA estimation accuracy. The selection of cost function is not within the scope of this paper. We use cross correlation as the cost function in the paper. In order to avoid optimum, an iterative checking strategy is introduced in this paper. Only the solution within the model error can be as feasible DOA. Otherwise, it needs to transform the switch selection combination to recalculate the DOA.

We present a detailed fitting strategy analysis here. According to the measurement model (referring to Equation (3)), if the true direction of the source is θ, the noise of each array element at the sampling time is of Gaussian distribution with zero mean and variance σ^2, i.e.,

$$n_m(t) \sim N\left[0, \sigma^2\right] \quad (m = 1, 2, \ldots, M) \tag{12}$$

Vector representation of DF array output is

$$\mathbf{y} = \mathbf{a}(\theta) \cdot s(t) + \mathbf{n}(t) \tag{13}$$

where

$$\mathbf{a} = [a_1(\theta), a_2(\theta), \ldots, a_M(\theta)]^T \tag{14}$$

$$\mathbf{n}(t) = [n_1(t), n_2(t), \ldots, n_M(t)]^T \tag{15}$$

We denote $\hat{\mathbf{y}}$ and $\hat{\theta}$ as the actually measured observation sample and the estimated value of the correlation matching, respectively. Provided that the estimated DOA is the same as the truth DOA (i.e., $\hat{\theta} = \theta$), then we have

$$\|\hat{y} - a(\theta) \cdot s(t)\|_2 = \|n(t)\|_2 \tag{16}$$

Considering the discrete lattice effect, the actual angle is just located at the lattice point with a probability of approximately zero. So, inequation $\hat{\theta} \neq \theta$ holds with a probability of approximately one. Further, we denote Δe as the residual of the model. Then, we have

$$\left\|\hat{\mathbf{y}} - \mathbf{a}\left(\hat{\theta}\right) \cdot s(t) + \Delta\mathbf{e}\right\|_2 = \|\mathbf{n}(t)\|_2 \tag{17}$$

$$\|\mathbf{n}(t)\|_2 - \|\Delta\mathbf{e}\| \leq \|\hat{\mathbf{y}} - \mathbf{a}(\theta) \cdot s(t)\|_2 \tag{18}$$

$$\|\hat{\mathbf{y}} - \mathbf{a}(\theta) \cdot s(t)\|_2 \leq \|\mathbf{n}(t)\|_2 + \|\Delta\mathbf{e}\|_2 \tag{19}$$

Equation (17) holds if and only if the estimated DOA is the same as the truth DOA. The greater the deviation of the estimated DOA $\hat{\theta}$ and the actual DOA θ is, the bigger model error is. Therefore, DOA can be estimated by setting the threshold $\hat{\theta}$ to make the true direction of the source and the estimated direction as close as possible.

It should be pointed out that the model residual tends to be 0 when $\hat{\theta} \to \theta$. So, we have following formula around the actual direction θ of the source.

$$\left\|\hat{\mathbf{y}} - \mathbf{a}\left(\hat{\theta}\right) \cdot s(t)\right\|_2 \approx \|\mathbf{n}(t)\|_2 \tag{20}$$

Further, taking account of the fact that each channel noise is i.i.d., we have

$$\frac{\left\|\hat{\mathbf{y}} - \mathbf{a}\left(\hat{\theta}\right) \cdot s(t)\right\|_2^2}{\sigma^2} \approx M \tag{21}$$

Since each component in $\mathbf{n}(t)$ is normal distribution with mean 0 and variance σ^2, we have

$$\frac{\left\|\hat{\mathbf{y}} - \mathbf{a}\left(\hat{\theta}\right) \cdot s(t)\right\|_2^2}{\sigma^2} = \frac{1}{\sigma^2}\sum_{k=1}^{M} n_k^2 \sim \aleph(M) \tag{22}$$

$\aleph(M)$ is the chi-square distribution with freedom degree M. Further, we define another variable

$$\xi \triangleq \frac{1}{\sigma^2}\sum_{k=1}^{M} n_k^2 \tag{23}$$

The p.d.f. of variable ξ is

$$p(\xi; M) = \begin{cases} \dfrac{\xi^{(M/2-1)}\exp^{(-M/2)}}{2^{M/2}\Gamma(M/2)} & \xi \geq 0 \\ 0 & \text{otherwise} \end{cases} \tag{24}$$

where $\Gamma(M/2)$ is Gamma function. The threshold of different confidence levels w.r.t. different freedom degrees can be calculated by numerical calculation or checking existing table. Specifically, when $M = 9$, the confidence probability is 0.99, and the value of integral argument is $\xi = 2.088$. We have

$$P\left(\frac{1}{\sigma^2}\sum_{k=1}^{9} n_k^2 > 2.088\right) = 0.99 \tag{25}$$

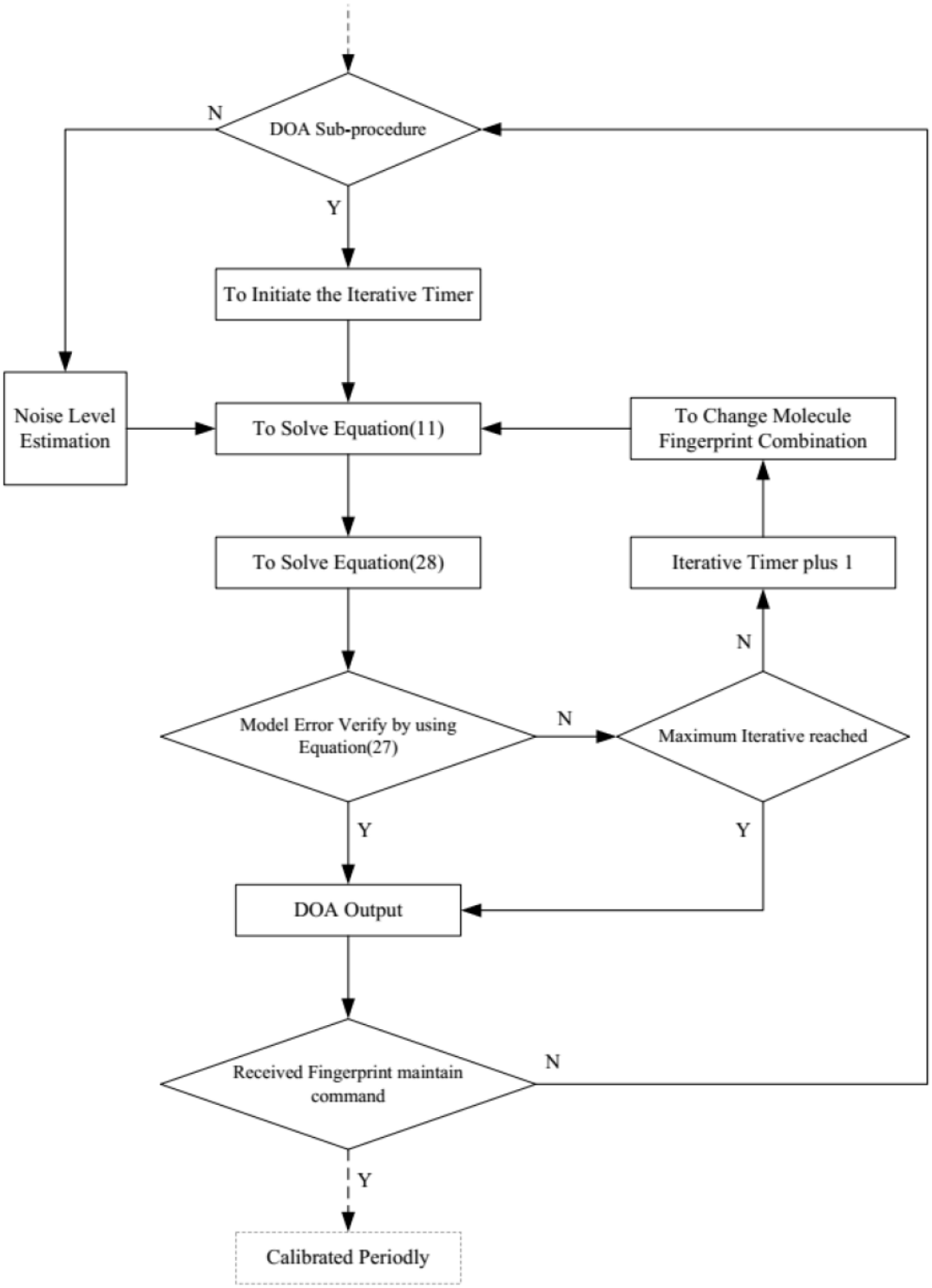

FIGURE 4. Flow chart of the proposed iterative algorithms. (The function of the first conditional block in figure is as a part of DF system, which is equivalent of DOA enable.)

So, the inequality $\|n(t)\|_2^2 > 2.088 \cdot \sigma_2$ holds with a probability of 0.99. Using Equation (18) and Equation (19), we have

$$1.445\sigma - \|\Delta\mathbf{e}\|_2 \leq \left\|\hat{\mathbf{y}} - \mathbf{a}\left(\hat{\theta}\right) \cdot \hat{s}(t)\right\|_2 \leq 1.445\sigma + \|\Delta\mathbf{e}\|_2 \tag{26}$$

Then, the following inequalities hold true.

$$\left|\left\|\hat{\mathbf{y}} - \mathbf{a}\left(\hat{\theta}\right) \cdot \hat{s}(t)\right\|_2 - 1.445\sigma\right| \leq \|\Delta\mathbf{e}\|_2 \tag{27}$$

In the inequality above, $\hat{s}(t)$ can be evaluated by using the least square method according to the observation vector and the array steering vector. i.e.,

$$\hat{s}(t) = \mathbf{a}^{+}(\theta) \cdot \hat{y} \tag{28}$$

In Equation (28), $\mathbf{a}^{+}(\theta)$ is the Pseudo-inverse of $\mathbf{a}(\theta)$. When the DOA of source is the same as the estimated version, the residual of model will be minimum. So the residual value of the actual model is very small. Without loss of generality, we set $\|\Delta e\|_2 = 0.001$. The parameter σ can be determined according to the actual statistics of system.

To avoid infinite loop, the maximum number of iterations is set in advance. The maximum number of iterations is not more than the number of combinations. For example, for DF system with 9 elements and each of the three elements been grouped together, the are totally $\mathbf{C}_9^3$ possible combinations. Once the maximum iteration number been reached, loop procedure stopped. The specific iterative flow chart is shown in Figure 4. As shown in the diagram, when DF instruction received, the maximum iterations and the maximum fitting residuals are calculated according to the actual measured noise intensity. Meanwhile, the received data and the fingerprint library are used to determine the possible DOA. And then the model residual is determined by using the estimated DOA and observation model of DF system. Either the model residuals are no more than fitting residuals or a maximum number of iterations reached, iteration procedure stopped. Otherwise, select another 3-channel combination for next iteration procedure and run the loop procedure again.

Remark 3.1. *The iterative method proposed in this paper is essentially a simplified version of the weighted iterative least squares (WILS) algorithm. As it is more concerned with engineering applications of the proposed method rather than its mathematical theory, the rationality of the method is proved through computer simulation. The rationality analysis of the proposed method is given based on model fitting error. In fact, the iterative threshold technique is often used in the fields of optimization theory, numerical computation, statistical signal processing, and so on. The specific content of the WILS method and its application can be found in* [13, 14].

3.3. **Sample database update.** In the ultra-small aperture DF system, the key issue of DOA is to use the difference between channels. To obtain good DOA accuracy with the proposed DF system, several constraints must be considered. Firstly, there must be differences between channels, which reduce the designing difficulty greatly. Secondly, the difference between channels must be known, which can be obtained accurately by building fingerprint database. Thirdly, in order to make the DF system adapt to the environment changes, sample database needs to be maintained dynamically. So real-time correction is required.

It should be pointed out that, there are a variety of rules for periodic correction. The fingerprints database can be calibrated at specified intervals, or corrected itself adaptively according to requirements. In this paper, the fingerprints will be built at the beginning, and then be periodically corrected by timer.

4. **Simulation.** A non-uniform linear array of 9 elements is used in this section. The effectiveness of the algorithm is verified by several computer simulation experiments.

Example 4.1. *In this experiment, positions of array elements in Cartesian coordinate (unit: mm) are* $(0, 0)$, $(0, 59.2)$, $(0, 99.8)$, $(0, 209.2)$, $(0, 282.8)$, $(0, 372.7)$, $(0, 524.2)$,

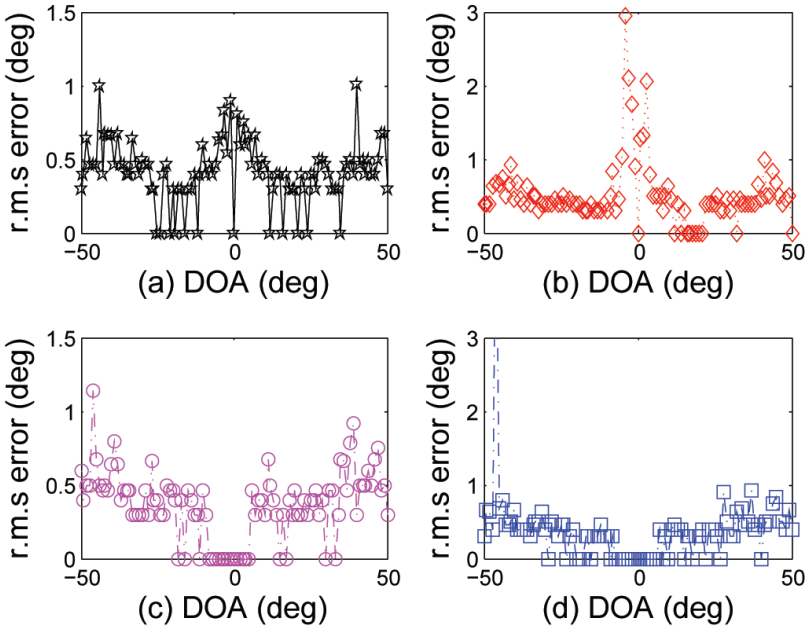

FIGURE 5. DOA error (r.m.s) vs. each angle (aperture to wave length ratio is 1)

$(0, 432.7)$ *and* $(0, 594.8)$*, respectively. The frequency of source and its bandwidth are 500MHz and 20MHz, respectively. The DOA of source ranges from* -50 *degree to 50 degree (namely,* $\theta_{\min}$ *and* $\theta_{\max}$ *in Equation (5) are* -50 *degree and 50 degree, respectively). The ideal pattern of each array element is predefined and noise level (i.e., signal-to-noise ratio) is 18dB. The number of snapshot is 32. 100 Monte Carlo trails is implemented to illustrate the effects of both channel inconsistency and the frequency measurement error versus DOA accuracy. Results of simulations are shown in Figure 5.*

In Figure 5(a), we assume that there are no amplitude error and phase error between channels. Meanwhile, there is also no frequency measurement error. In Figure 5(b), just frequency measurement error about is of 200KHz. From the two subplots, we can see that frequency measurement error has a limited influence on DOA accuracy. In Figure 5(c), both amplitude and phase error are considered. Amplitude difference and phase jitter range are 1dB and 10°, respectively. Contrasting Figure 5(a) and Figure 5(c), the DOA accuracy is similar to that of the ideal scenario. This shows that channel errors have few effects on the DOA accuracy. In Figure 5(d), amplitude error, phase error, as well as frequency measurement errors are all considered. The amplitude error, the phase error, and frequency measurement error are 1dB, 10°, and 200KHz, respectively. Comparing the left upper subplot and the right lower subplot, we can see that the proposed algorithm has the same DOA accuracy as the interferometer.

Example 4.2. *In this experiment, positions of array elements in Cartesian coordinate (unit: mm) are* $(0, 0)$*,* $(0, 11.3)$*,* $(0, 22.5)$*,* $(0, 33.8)$*,* $(0, 45)$*,* $(0, 56.2)$*,* $(0, 67.5)$*,* $(0, 78.8)$*, and* $(0, 90)$*, respectively. The carrier frequency of source and its bandwidth are 500MHz and 20MHz, respectively. The DOA of source ranges from* -50 *degree to 50 degree. The ideal pattern of each array element is supposed and noise level is 18dB. The number of snapshot is also 32. We demonstrate the effects of both channel inconsistency and the frequency measurement error versus DOA accuracy with the ultra-small aperture DF system. 100 Monte Carlo trails is implemented in simulation. Results of simulations are shown in Figure 6.*

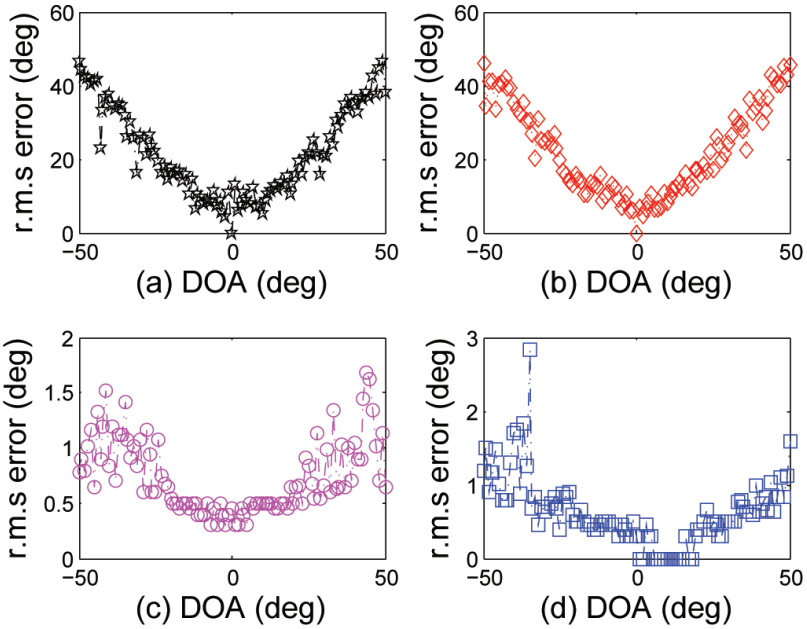

FIGURE 6. DOA error (r.m.s) vs. each angle (aperture to wave length ratio is 0.15)

In Figure 6(a), we assume that there are no amplitude error and phase error between channels. Meanwhile, there is also no frequency measurement error. The results of simulation demonstrate that the DOA accuracy is a function of angle. Once the source deviates from broadside of the array, the DOA accuracy deteriorates dramatically. This is because the DOA accuracy is determined by DF array aperture under ideal scenario.

In Figure 6(b), just frequency measurement error is about of 200KHz. Figure 6(a) and Figure 6(b) show that frequency measurement error has a limited influence on DOA accuracy. This is similar to the traditional interferometer DF system. In Figure 6(c), both amplitude and phase error are considered. Amplitude difference and phase jitter range are 1dB and 10°, respectively. Comparing the left upper subplot and left lower subplot, we can see that in each angle, the DOA accuracy is significantly improved compared with the ideal situation. The simulation results show that aperture limit can be exceeded if the channel error is introduced into the database as a priori information in the ultra-small aperture DF system with the proposed algorithm. It should be pointed out that DOA accuracy is limited by aperture-to-wavelength ratio with traditional interferometer. However, with the proposed algorithm, this drawback is solved perfectly. In the right lower subplot, amplitude error, phase error, as well as frequency measurement errors are all considered. The amplitude error, the phase error, and frequency measurement error are 1dB, 10°, and 200KHz, respectively. The results in Figure 6(d) show that the non-ideal factors are a burden to obtain DOA in traditional interferometer, but it is a welfare for the ultra-small aperture DF system.

Example 4.3. *In order to illustrate the practical significance of the proposed algorithm, the DOA accuracy is verified by introducing a practical array pattern in this experiment. The pattern of each element ranges from −50 degree to 50 degree, which is shown in Figure 7. The other parameters are set as the same as those in Example 4.2. The simulation results are presented in Figure 8.*

In Figure 8(a), we assume that there are no amplitude error and phase error between channels. Meanwhile, there is also no frequency measurement error but the actual antenna

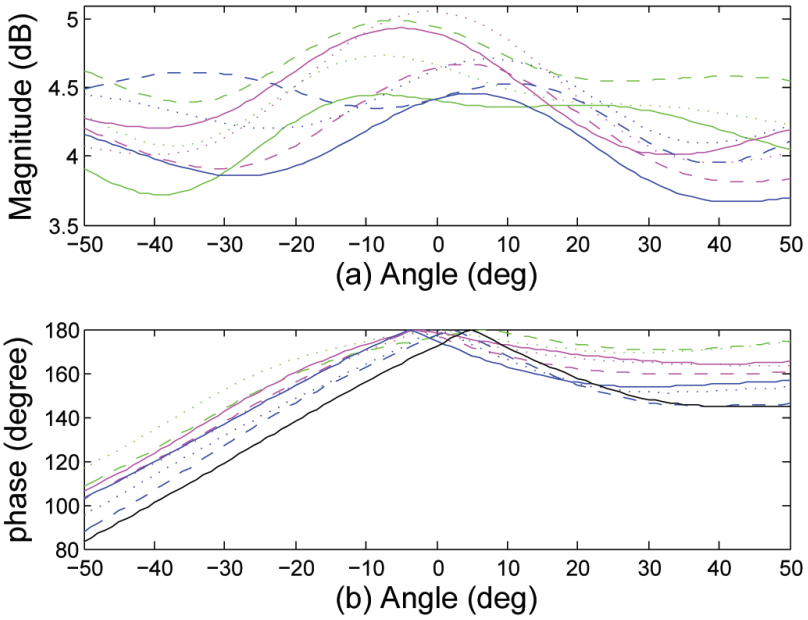

FIGURE 7. 9 elements pattern (magnitude for upper and phase for bottom)

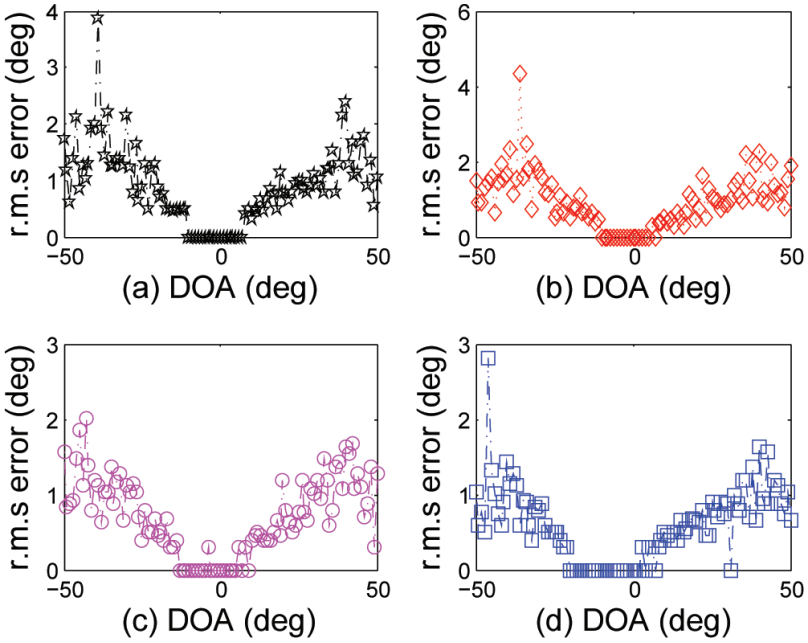

FIGURE 8. DOA error (r.m.s) vs. each angle with practical antenna array

pattern shown in Figure 8 is introduced. In Figure 8(b), we only consider the frequency measurement error round 200KHz. The two figures show that frequency measurement error has a limited influence on DOA accuracy.

In Figure 8(c), both amplitude and phase error are considered. Amplitude difference and phase jitter range are 1dB and 10° respectively. Contrasting Figure 8(a) and Figure 8(c), the DOA accuracy has been further improved. This is because that the difference of fingerprint database in the ultra-small aperture system not only contains the antenna pattern, but also errors of among channels, which are equivalent to increasing the amount of information of the fingerprint database. Therefore, it can improve DOA accuracy. With the proposed algorithm, it can break through the restrictions on DF aperture by high

precision measurement. In the right lower subplot, amplitude error, phase error, as well as frequency measurement errors are all considered. The amplitude error, the phase error, and frequency measurement error are 1dB, 10°, and 200KHz, respectively. The results show that the influence of frequency error versus the DOA accuracy is limited for the actual antenna array. Meanwhile, the results also show that the DOA accuracy with the proposed algorithm is approximate to the medium aperture.

Remark 4.1. *It needs to be pointed out that, on the one hand, DF array types are very flexible because of cross correlation operation introduced in the proposed algorithm, which can adapt to different structures of the platform. Meanwhile, due to the fact that the non-ideal errors of the systems such as mutual coupling among array elements, errors of magnitude and phase among channels are known information in the proposed algorithm, our method shows better adaptable ability to different environments. As a contrast, fussy calibrations must be provided in traditional solutions.*

On the other hand, since the sample data of 9 elements is obtained by 3-channels receivers, the proposed method could reduce the hardware cost of DF system without loss of the amount of information. The DOA accuracy of ultra-small aperture is approximately same as the medium aperture ones. What is more, it is insensitive to source type of signal. If the iteration number in Figure 4 is set to 1, the proposed method degrades to the traditional correlation interferometer automatically.

Example 4.4. *In order to compare the advantages of the proposed algorithm in this paper with the traditional one (referring to* [12]*), we simulate the angle measurement accuracy for different snapshots. In the experiment, amplitude errors among channels and phase jitter are 1dB and 10 degree respectively. The maximum error of the estimated frequency is within 200KHz. The distance among the elements is the same as in Example 4.2. The DOA of source increased from −50 degree to 50 degree. The discrete angle interval of the sample library is 1°. The noise level (i.e., signal to noise ratio) is 18dB. The simulation results with 100 Monte Carlo trials are shown in Figure 9. In the figure, the dotted line is the traditional method proposed in* [13]*, and the solid line is the proposed algorithm in this paper. Simulation results show that the proposed method has better performance than the traditional method in ultra-small aperture.*

Example 4.5. *In order to illustrate the advantages of the proposed algorithm in detail, we also simulate the angle measurement accuracy for different noise levels. In simulations, amplitude errors among channels and phase jitter as well as the errors of the estimated frequency of source are set the same as in Example 4.4. The distance among the elements is the same as in Example 4.2. The DOA of source is increased from −50 degree to 50 degree. The discrete angle interval of the sample library is 1°. The number of snapshots is 32. The simulation results with 100 Monte Carlo trials are shown in Figure 10. According to the simulation results, our method outperforms the traditional one in ultra-small aperture case.*

5. **Conclusion.** In the conventional DF solutions, reducing DF aperture will lead to the degradation of DOA accuracy. In this paper, we propose a strategy to obtain high-dimensional fingerprint database by switching sampling mode in low-dimensional measurement array elements. DOA of source is recovered by correlation operation in high-dimensional fingerprint database which contains fingerprint features of all non-ideal factors. An iterative algorithm is proposed for ultra-small aperture DF system, which breaks through the traditional array aperture requirement. One drawback of the proposed method is that it cannot separate multiple signals in the same frequency. To make

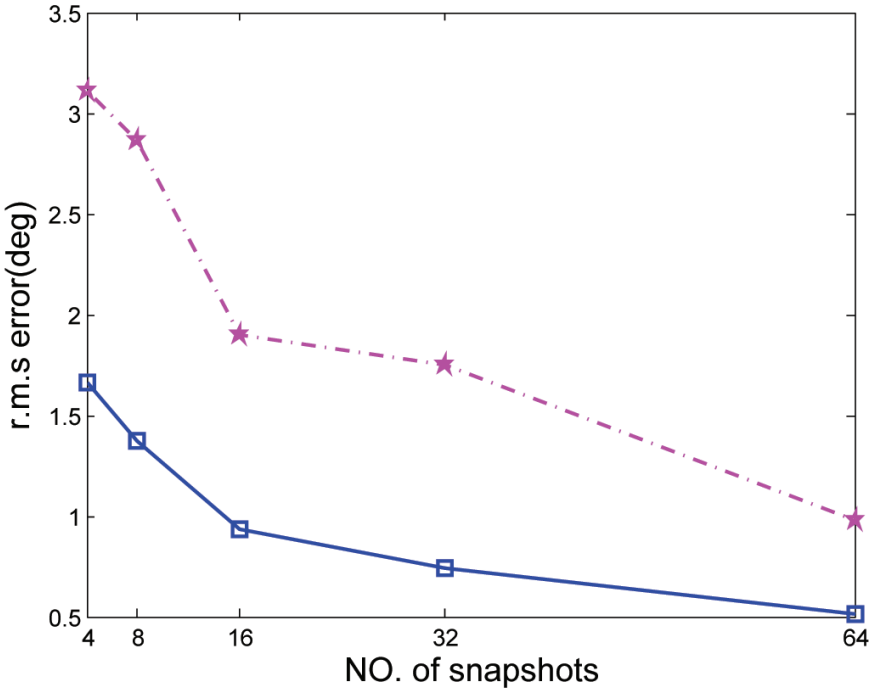

FIGURE 9. DOA error (r.m.s) vs. snapshot number

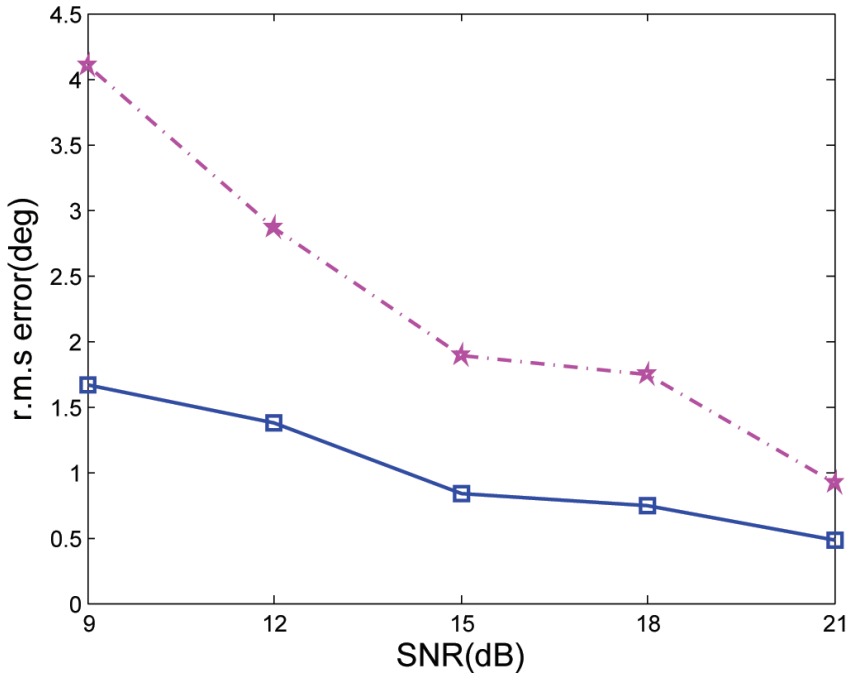

FIGURE 10. DOA error (r.m.s) vs. noise SNR

up this drawback, we will continue our research on how to generalize the method to estimating DOA in multi-path environment.

Acknowledgment. This work was supported in part by the National Natural Science Foundation of China (NSFC) under Grant U1533125, National Science and Technology Major Project (2016ZX03001022). This work was also supported in part by the Open

Foundation of CETC Key Laboratory of Avionic Information System Technology under Grant H15009.

REFERENCES

[1] X. C. Cong, G. Gui, X. Li, G. J. Wen, X. H. Huang and Q. Wan, Object-level SAR imaging method with canonical scattering characterization and inter-subdictionary interferences mitigation, *IET Radar, Sonar & Navigation*, vol.10, pp.784-790, 2016.

[2] H. Krim and M. Viberg, Two decades of array signal processing research: The parametric approach, *IEEE Signal Processing Magazine*, vol.13, pp.67-94, 1996.

[3] C. Zhang and Y. Pang, Joint DOD and DOA estimation in bistatic MIMO radar with sparse linear array, *ICIC Express Letters, Part B: Applications*, vol.5, no.4, pp.933-938, 2014.

[4] Q. He, Z. S. He and H. Y. Li, Multibeam amplitude comparison problems for MIMO radar's angle measurement, *Record of the 41st Asilomar Conference on Signals, Systems and Computers*, pp.2163-2167, 2007.

[5] J. Chen, D. H. Liu and P. Liu, Amplitude-comparison angle measurement methods of passive phased array radar at different SNRs, *RADAR & ECM*, vol.35, pp.28-37, 2015.

[6] Z. F. Zhang and Q. Qiao, Direction of finding processing method of correlation interferometer under low SNR, *Shipboard Electronic Countermeasure*, vol.32, pp.103-106, 2009.

[7] X. W. Chen, Y. Z. Li and G. Y. Zhang, Error analysis of measuring direction of LFM signal using interferometer, *Journal of Sichuan Ordnance*, vol.8, pp.119-123, 2015.

[8] P. Stoica and A. Nehorai, MUSIC, maximum likelihood and Cramer-Rao bound, *IEEE Trans. Acoust., Speech, Signal Process.*, vol.37, pp.720-741, 1989.

[9] F. Wen, Q. Wan, R. Fan et al., Improved MUSIC algorithm for multiple noncoherent subarrays, *IEEE Signal Processing Letters*, vol.21, pp.527-530, 2014.

[10] G. Berk, Particle velocity gradient based acoustic mode beamforming for short linear vector sensor arrays, *Journal of Acoustical Society of America*, vol.135, pp.3463-3473, 2014.

[11] X. J. Guo, S. Yang and S. Miron, Low-frequency beamforming for a miniaturized aperture three-by-three uniform rectangular array of acoustic vectors sensors, *Journal of Acoustical Society of America*, vol.138, pp.3873-3883, 2015.

[12] H. W. Wei, J. Wang and S. F. Ye, An algorithm of estimation direction of arrival for phase interferometer array using cosine function, *Journal of Electronics and Information Technology*, vol.29, pp.2665-2668, 2007.

[13] I. Daubechies, R. Devore and M. Fornasier, Iteratively reweighted least squares minimization for sparse recovery, *Communications on Pure and Applied Mathematics*, vol.63, pp.1-38, 2008.

[14] Z. Lu, Iterative hard thresholding methods for l_0 regularized convex cone programming, *Mathematical Programming*, vol.147, pp.125-154, 2014.